The CMB temperature bispectrum induced by cosmic strings

Article (Published Version)

PHYSICAL REVIEW D **80,** 083501 (2009)

CMB temperature bispectrum induced by cosmic strings

Mark Hindmarsh*
Department of Physics & Astronomy, University of Sussex, Brighton, BN19QH, United Kingdom

Christophe Ringeval† and Teruaki Suyama‡
Theoretical and Mathematical Physics Group, Centre for Particle Physics and Phenomenology, Louvain University, 2 Chemin du Cyclotron, 1348 Louvain-la-Neuve, Belgium
(Received 6 August 2009; published 2 October 2009)

The cosmic microwave background (CMB) bispectrum of the temperature anisotropies induced by a network of cosmic strings is derived for small angular scales, under the assumption that the principal cause of temperature fluctuations is the Gott-Kaiser-Stebbins effect. We provide analytical expressions for all isosceles triangle configurations in Fourier space. Their overall amplitude is amplified as the inverse cube of the angle and diverges for flat triangles. The isosceles configurations generically lead to a negative bispectrum with a power-law decay ℓ^{-6} for large multipole ℓ. However, collapsed triangles are found to be associated with a positive bispectrum whereas the squeezed triangles still exhibit negative values. We then compare our analytical estimates to a direct computation of the bispectrum from a set of 300 statistically independent temperature maps obtained from Nambu-Goto cosmic string simulations in a Friedmann-Lemaître-Robertson-Walker universe. We find good agreement for the overall amplitude, the power-law behavior, and the angle dependency of the various triangle configurations. At $\ell \sim 500$ the cosmic string Gott-Kaiser-Stebbins effect contributes approximately the same equilateral CMB bispectrum amplitude as an inflationary model with $|f_{\rm NL}^{\rm loc}| \simeq 10^3$, if the strings contribute about 10% of the temperature power spectrum at $\ell = 10$. Current bounds on $f_{\rm NL}$ are not derived using cosmic string bispectrum templates, and so our $f_{\rm NL}$ estimate cannot be used to derive bounds on strings. However it does suggest that string bispectrum templates should be included in the search of CMB non-Gaussianities.

DOI: 10.1103/PhysRevD.80.083501 PACS numbers: 98.80.Cq, 98.70.Vc

I. INTRODUCTION

Cosmic strings are linelike objects formed in the early universe [1–3]. They could be solitons in field theories with spontaneously broken symmetries [4], singular solutions with cylindrical symmetry in supergravity theories [5], or fundamental objects in string theory [6]. They may form in thermal phase transitions [4], at the end of hybrid inflation [7–10], or by tachyon condensation at the end of brane inflation when brane and antibrane annihilate [11,12]. If cosmic strings are added to the standard power-law ΛCDM model, the cosmic microwave background (CMB) data are fitted even better [13,14] if the fraction of the temperature power spectrum (at $\ell = 10$) due to strings f_{10} is about 0.1. There is therefore strong motivation to develop further tests for strings in future CMB data, which provide the cleanest and best understood cosmological string signals [15–17]. Calculations of the polarization B mode [18,19] show that a promising line of attack for the near future is to look for a signal peaked between $\ell = 600$–1000. Simulations of Planck data show that it will be sensitive down to $f_{10} \simeq 0.01$, and that there is no danger of confusing strings with inflationary tensor perturbations [18]. Perhaps the most characteristic signal in the CMB comes from the Gott-Kaiser-Stebbins (GKS) effect [20,21], which is due to the gravitational lensing of photons passing near a moving string. This produces a discontinuity in the apparent temperature approximately proportional to the transverse velocity of the string v and the string tension U:

$$\delta T \sim 8\pi(GU)vT_{\rm CMB}, \tag{1}$$

where G is Newton's constant. Given that strings move with a mean square (rms) velocity of between 0.25 and 0.36 [22,23], we would expect to see discontinuities δT of up to about 1 μK. Recent calculations of the integrated Sachs-Wolf CMB signal at small angular scales have shown that the angular power spectrum it produces decreases slowly, approximately $\ell^{-0.9}$ at high multipole moment ℓ [24]. If $f_{10} \simeq 0.1$ strings should dominate the adiabatic temperature power spectrum for $\ell \gtrsim 3000$, and remain above the thermal Sunyaev-Zel'dovich effect. This fraction corresponds to $GU \simeq 0.7 \times 10^{-6}$ for strings in the Abelian Higgs model [14]. The slow power-law decrease in the power spectrum is quite close to a prediction of the small-scale power spectrum using the string correlation functions in a Gaussian approximation [25], which gave a temperature anisotropy power going as ℓ^{-1}. The non-Gaussian nature of the maps exhibited in [24], as, for example, exhibited by the skewness of the distribution of the 1-point function [26], immediately motivates an attempt to generalize the calculation to higher-order correlators, and, in

*m.b.hindmarsh@sussex.ac.uk
†christophe.ringeval@uclouvain.be
‡teruaki.suyama@uclouvain.be

particular, the 3-point function or bispectrum, which will become increasingly well characterized by future CMB data [17,27–29]. This paper reports on the results of this calculation. It is found that the bispectrum for an isosceles arrangement of wave vectors $\boldsymbol{k}$ in Fourier space is generically negative and decreases as $|\boldsymbol{k}|^{-6}$. It is proportional to $(GU)^3$ and hence to the power spectrum raised to the $3/2$ power. The scale of the nonlinearity parameter $f_{\rm NL}$, defined by dividing the bispectrum by the square of the power spectrum, is therefore potentially large, going as $(GU)^{-1}$.

II. ANALYTICAL BISPECTRUM

A. Gott-Kaiser-Stebbins effect

We work in the flat sky approximation, and define transverse coordinates $\boldsymbol{x}$ measured in radians. The wave number $\boldsymbol{k}$ is related to the multipole moment ℓ by [30,31]

$$k^2 \simeq \ell(\ell+1). \tag{2}$$

The anisotropy power $\ell(\ell+1)C_\ell$ is then approximately equal to $k^2|\delta T_{\boldsymbol{k}}|^2$, where $\delta T_{\boldsymbol{k}}$ is the Fourier transform of the temperature fluctuation,

$$\delta T_{\boldsymbol{k}} = \int d\boldsymbol{x}\delta T e^{i\boldsymbol{k}\cdot\boldsymbol{x}}. \tag{3}$$

We will also define $\Theta(\boldsymbol{x}) = \delta T(\boldsymbol{x})/T_{\rm CMB}$. String spacetime coordinates will be denoted $X^\mu(\tau,\sigma)$, where τ and σ are timelike and spacelike world sheet coordinates, respectively. In the temporal gauge the $X^0 = \tau$ (where the world sheet time is identified with the background time coordinate) (corrected) GKS formula is [25]

$$\boldsymbol{\nabla}^2\Theta = -8\pi GU\int d\sigma\left[\dot{\boldsymbol{X}} - \frac{(\acute{\boldsymbol{X}}\cdot\hat{p})}{(\dot{\boldsymbol{X}}\cdot\hat{p})}\acute{\boldsymbol{X}}\right]\cdot\boldsymbol{\nabla}\delta^{(2)}(\boldsymbol{x}-\boldsymbol{X}), \tag{4}$$

where $\hat{p}^\mu = p^\mu/E$, and world sheet variables are evaluated at the retarded time $t_{\rm r} = t + z - X^3(\sigma, t_{\rm r})$, when the CMB photons (taken to be moving in the $-z$ direction) pass the string. The expression is greatly simplified in the light-cone gauge,

$$X^+(\sigma,\tau) = \tau, \tag{5}$$

where $X^\pm = X^0 \pm X^3$. The time parameter τ then labels the intersections with a set of null hyperplanes with the world sheet: the photon geodesics $Z^\mu = x^\mu + \lambda p^\mu$ form just such a set. Then we find

$$\boldsymbol{\nabla}^2\Theta = -8\pi GU\int d\sigma\dot{\boldsymbol{X}}\cdot\boldsymbol{\nabla}\delta^{(2)}(\boldsymbol{x}-\boldsymbol{X}), \tag{6}$$

where world sheet quantities are now evaluated at $\tau = x^+ = t + z$. In Fourier space the equation becomes

$$-k^2\Theta_{\boldsymbol{k}} = i\epsilon k_A\int d\sigma\dot{X}^A(\sigma)e^{i\boldsymbol{k}\cdot\boldsymbol{X}(\sigma)}, \tag{7}$$

where we have defined

$$\epsilon = 8\pi GU, \tag{8}$$

and $A = 1, 2$ with implicit summation on repeated indices. It is now clear that the power spectrum, bispectrum, and higher-order correlators can be evaluated in terms of correlation functions of the string network, as projected onto our backward light cone. In the next section we will introduce the relevant correlation functions and discuss their important features.

B. String correlation functions

We denote the transverse coordinates of the string, $X^A(\sigma)$. The basic two point functions are

$$\langle\dot{X}^A(\sigma)\dot{X}^B(\sigma')\rangle, \qquad \langle\dot{X}^A(\sigma)\acute{X}^B(\sigma')\rangle, \qquad \langle\acute{X}^A(\sigma)\acute{X}^B(\sigma')\rangle, \tag{9}$$

where the angle brackets denote an average over an ensemble of strings. The starting assumption is that the string ensemble is well approximated by a Gaussian process: that is, all correlators can be calculated in terms of the two point functions. We now make some assumptions about the ensemble: (i) rotation, reflection, and translation invariance of the transverse coordinates; and (ii) world sheet reflection and translation invariance. There are three independent correlation functions:

$$\langle\dot{X}^A(\sigma)\dot{X}^B(\sigma')\rangle = \tfrac{1}{2}\delta^{AB}V(\sigma-\sigma'), \tag{10}$$

$$\langle\acute{X}^A(\sigma)\acute{X}^B(\sigma')\rangle = \tfrac{1}{2}\delta^{AB}T(\sigma-\sigma'), \tag{11}$$

$$\langle\acute{X}^A(\sigma)\dot{X}^B(\sigma')\rangle = \tfrac{1}{2}\delta^{AB}M_1(\sigma-\sigma'). \tag{12}$$

A fourth,

$$M_2(\sigma) = \langle\dot{X}^A(\sigma)\acute{X}^B(0)\rangle\epsilon^{AB}, \tag{13}$$

vanishes because of the symmetry $X^1 \leftrightarrow X^2$ (this point was overlooked in Ref. [25]). The functions V and T are symmetric in their argument, while M_1 is antisymmetric. The forms of the correlators are sketched in Fig. 1 (see also [23]). For later convenience two other correlators will be defined:

$$\Gamma(\sigma-\sigma') \equiv \langle[\boldsymbol{X}(\sigma)-\boldsymbol{X}(\sigma')]^2\rangle \tag{14}$$

$$= \int_{\sigma'}^{\sigma}d\sigma_1\int_{\sigma'}^{\sigma}d\sigma_2 T(\sigma_1-\sigma_2), \tag{15}$$

$$\Pi(\sigma-\sigma') \equiv \langle[\boldsymbol{X}(\sigma)-\boldsymbol{X}(\sigma'))]\cdot\dot{\boldsymbol{X}}(\sigma')\rangle \tag{16}$$

$$= \int_{\sigma'}^{\sigma}d\sigma_1 M_1(\sigma_1-\sigma'). \tag{17}$$

There are integral constraints arising from the fact that the average velocity of the strings vanishes on large scale:

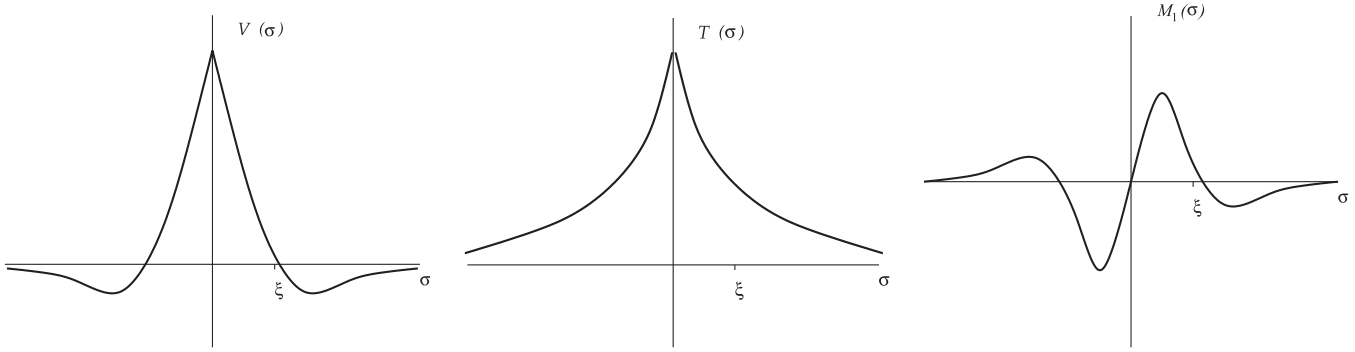

FIG. 1. Sketches of string correlation functions $V(\sigma)$ (velocity-velocity), $T(\sigma)$ (tangent-tangent), and $M_1(\sigma)$ (velocity-tangent), as a function of the string world sheet spacelike separation σ, defined in Eqs. (10)–(12).

$$\int d\sigma V(\sigma) \to 0, \qquad \int d\sigma M_1(\sigma) \to 0. \tag{18}$$

The important asymptotic forms are

$$V(\sigma) \to \begin{cases} \bar{v}^2 & \sigma \to 0, \\ \sigma \to 0 & \sigma \to \infty, \end{cases} \tag{19}$$

$$\Gamma(\sigma) \to \begin{cases} \bar{t}^2 \sigma^2 & \sigma \to 0, \\ \hat{\xi}\sigma & \sigma \to \infty, \end{cases} \tag{20}$$

$$\Pi(\sigma) \to \begin{cases} \frac{1}{2}\frac{c_0}{\hat{\xi}}\sigma^2 & \sigma \to 0, \\ 0 & \sigma \to \infty, \end{cases} \tag{21}$$

where we have defined four parameters

$$\hat{\xi} = \Gamma'(\infty), \tag{22}$$

$$\bar{v}^2 = \langle \dot{\boldsymbol{X}}^2 \rangle, \tag{23}$$

$$\bar{t}^2 = \langle \acute{\boldsymbol{X}}^2 \rangle, \tag{24}$$

$$c_0 = \hat{\xi}\langle \acute{\boldsymbol{X}} \cdot \dot{\boldsymbol{X}} \rangle. \tag{25}$$

The correlation length $\hat{\xi}$ is the projected correlation length on the backward light cone, $\bar{t}^2$ is the mean square projected tangent vector (of order unity), $\bar{v}^2$ is the mean square projected velocity (again of order unity), and c_0 is the correlation between the projected velocity and curvature.

C. Light-cone gauge equations

In Minkowski space, the Nambu-Goto action leads to the equations of motion and constraints

$$\ddot{X}^\mu - \acute{\dot{X}}^\mu = 0, \qquad \dot{X}^2 + \acute{X}^2 = 0, \qquad \dot{X} \cdot \acute{X} = 0. \tag{26}$$

The light-cone gauge consists of choosing $\tau = X^+ = X^0 + X^3$. Hence

$$\dot{X}^- = \dot{X}_A \dot{X}^A + \acute{X}_A \acute{X}^A, \qquad \acute{X}^- = 2\dot{X}_A \acute{X}^A. \tag{27}$$

The equations of motion in a Friedmann-Lemaître-Robertson-Walker (FLRW) background follow from the Nambu-Goto action

$$S = -U \int d\tau d\sigma \sqrt{-\gamma} = -U \int d\tau d\sigma a^2(X^0) \sqrt{-\dot{X}^2 \acute{X}^2 + (\dot{X} \cdot \acute{X})^2}, \tag{28}$$

where γ is the determinant of the induced metric along the string world sheet, and $a(X^0)$ is the scale factor. With the standard gauge choice $\dot{X} \cdot \acute{X} = 0$, we find

$$\ddot{X}^\mu + \left(\frac{\dot{\varepsilon}}{\varepsilon} + 2\frac{\dot{a}}{a}\right)\dot{X}^\mu - \frac{1}{\varepsilon}\frac{\partial}{\partial\sigma}\left(\frac{1}{\varepsilon}\frac{\partial X^\mu}{\partial\sigma}\right) - 2\frac{1}{a}\frac{da}{dX^0}\frac{1}{\varepsilon}\frac{\partial X^0}{\partial\sigma} \times \frac{1}{\varepsilon}\frac{\partial X^\mu}{\partial\sigma} + 2\delta^\mu_0 \frac{1}{a}\frac{da}{dX^0}\dot{X}^2 = 0, \tag{29}$$

where $\varepsilon = \sqrt{-\acute{X}^2/\dot{X}^2}$. The light-cone gauge choice $X^+ = \tau$ produces as the equation of motion for X^+

$$\frac{\dot{\varepsilon}}{\varepsilon} + 2\mathcal{H}(\dot{X}^0 + \dot{X}^2) = 0, \tag{30}$$

where $\mathcal{H} = d\ln a/dX^0$ is the conformal Hubble parameter. The equation for the transverse components is

$$\ddot{\boldsymbol{X}} + 2\mathcal{H}\frac{1}{\varepsilon^2}(\acute{\boldsymbol{X}}^2)\dot{\boldsymbol{X}} - \frac{1}{\varepsilon}\frac{\partial}{\partial\sigma}\left(\frac{1}{\varepsilon}\frac{\partial \boldsymbol{X}}{\partial\sigma}\right) - 2\mathcal{H}\frac{1}{\varepsilon^2}(\dot{\boldsymbol{X}} \cdot \acute{\boldsymbol{X}})\acute{\boldsymbol{X}} = 0. \tag{31}$$

In a FLRW background, assuming that $\langle \dot{\boldsymbol{X}}^2 \rangle$ is constant, and neglecting higher-order correlations between $\mathcal{H}$, $\dot{\boldsymbol{X}}$, and $\acute{\boldsymbol{X}}$, we find

$$\left\langle \frac{\partial^2 \boldsymbol{X}}{\partial s^2} \cdot \dot{\boldsymbol{X}} \right\rangle = 2\bar{\mathcal{H}}\left\langle \left(\frac{\partial \boldsymbol{X}}{\partial s}\right)^2 \dot{\boldsymbol{X}}^2 \right\rangle - 2\bar{\mathcal{H}}\left\langle \left(\dot{\boldsymbol{X}} \cdot \frac{\partial \boldsymbol{X}}{\partial s}\right)^2 \right\rangle, \tag{32}$$

where we have defined $ds = \varepsilon d\sigma$, and where $\bar{\mathcal{H}}$ is the conformal Hubble parameter averaged over the string ensemble at fixed $\tau = X^+$, which will select the value where there is the most string, i.e. at decoupling.

If we assume that the string ensemble is approximately Gaussian in $\dot{\boldsymbol{X}}$ and $\acute{\boldsymbol{X}}/\varepsilon$, it is not hard to show that the right-

hand side reduces to

$$\left\langle \frac{\partial^2 \boldsymbol{X}}{\partial s^2} \cdot \dot{\boldsymbol{X}} \right\rangle = \bar{\mathcal{H}}(\langle \dot{\boldsymbol{X}}^2 \rangle \langle \acute{\boldsymbol{X}}^2 \rangle - \langle \dot{\boldsymbol{X}} \cdot \acute{\boldsymbol{X}} \rangle^2). \tag{33}$$

The last term vanishes, so the cross correlator simplifies to $\bar{\mathcal{H}}\bar{v}^2\bar{t}^2$ which is positive. From Eq. (25), one gets that in a FLRW background, a string network should exhibit $c_0 > 0$. We see also that it vanishes in Minkowski space, which can be viewed as a consequence of time-reversal invariance. As shown in the next sections, the temperature bispectrum vanishes when the correlator Π does, and so the generation of a bispectrum by strings simply requires the breaking of time-reversal invariance, as it is in a FLRW background.[1]

D. Temperature power spectrum at small angular scales

The power spectrum at small angular scales, where the GKS effect [20,32] is held to be dominant, was calculated in Ref. [25], and the calculation is recapped here for completeness. The Fourier transform of the temperature fluctuation given in Eq. (6) reads

$$\Theta_{\boldsymbol{k}} = \int d^2x \frac{\delta T}{T} e^{i\boldsymbol{k}\cdot\boldsymbol{x}}, \tag{34}$$

and hence is given by Eq. (7). The power spectrum is defined by

$$\langle \Theta_{\boldsymbol{k}_1} \Theta_{\boldsymbol{k}_2} \rangle = P(k_1)(2\pi)^2 \delta(\boldsymbol{k}_1 + \boldsymbol{k}_2). \tag{35}$$

With our conventions we need a box of formal area $\mathcal{A} = (2\pi)^2\delta(0)$ to express the power spectrum

$$P(k) = \epsilon^2 \frac{k_A k_B}{Ak^4} \int d\sigma d\sigma' \langle \dot{X}^A(\sigma) \dot{X}^B(\sigma') e^{i\boldsymbol{k}\cdot[\boldsymbol{X}(\sigma) - \boldsymbol{X}(\sigma')]} \rangle. \tag{36}$$

With our assumptions about the string correlation functions, the ensemble average can be reduced to

$$P(k) = \frac{1}{2}\varepsilon^2 \frac{1}{\mathcal{A}k^2} \int d\sigma d\sigma' [V(\sigma - \sigma') + \frac{1}{2}k^2 \Pi^2(\sigma - \sigma')] e^{-k^2\Gamma(\sigma - \sigma')/4}. \tag{37}$$

We now derive the asymptotic behavior of $P(k)$ as $(k\xi)$ gets large. The contribution to the power spectrum from the mixed correlator M_1 can be shown to be subdominant at high k [25], and so we need to examine only the first term in the power spectrum of Eq. (37),

$$P(k) = \varepsilon^2 \frac{1}{4\mathcal{A}k^2} \int d\sigma_+ d\sigma_- V(\sigma_-) e^{-k^2\Gamma(\sigma_-)/4}, \tag{38}$$

where $\sigma_\pm = \sigma \pm \sigma'$. For $k\hat{\xi} \gg 1$, we find

$$k^2 P(k) \simeq \varepsilon^2 \sqrt{\pi} \frac{L\hat{\xi}}{\mathcal{A}} \frac{\bar{v}^2}{\bar{t}} \frac{1}{(k\hat{\xi})}, \tag{39}$$

where L is the total transverse light-cone gauge length of string in the box of area $\mathcal{A}$.

The power spectrum given in Ref. [33] was consistent with k^{-1}, and the amplitude was surprisingly close for such a crude estimate. Fraisse *et al.* [24] have a slightly different small-scale angular power spectrum: $k^2P(k) \sim k^{-p}$ with $p \simeq -0.89$. This can be explained if $\Gamma(\sigma) \sim \sigma^{2/p}$ on the relevant scales. This correlation function controls how far on average one moves in the transverse coordinates as one moves along the string: $p = 1$ would correspond to straight lines, while $p = 2$ to a Brownian random walk. A power less than 1 is suggestive of a cloud of zero-dimensional objects along the string world sheet which may be the signature of small loop production.

E. Temperature bispectrum from strings at small angular scales

In the flat sky approximation the three point temperature correlation function or bispectrum is defined as

$$\langle \Theta_{\boldsymbol{k}_1} \Theta_{\boldsymbol{k}_2} \Theta_{\boldsymbol{k}_3} \rangle = B(\boldsymbol{k}_1, \boldsymbol{k}_2, \boldsymbol{k}_3)(2\pi)^2 \delta(\boldsymbol{k}_1 + \boldsymbol{k}_2 + \boldsymbol{k}_3). \tag{40}$$

We again need to normalize by a formal area factor $\mathcal{A} = (2\pi)^2\delta(0)$ to obtain an expression in terms of a string expectation value

$$B(\boldsymbol{k}_1, \boldsymbol{k}_2, \boldsymbol{k}_3) = i\epsilon^3 \frac{1}{\mathcal{A}} \delta_{A\bar{A}}\delta_{B\bar{B}}\delta_{C\bar{C}} \frac{k_1^{\bar{A}} k_2^{\bar{B}} k_3^{\bar{C}}}{k_1^2 k_2^2 k_3^2} \times \int d\sigma_1 d\sigma_2 d\sigma_3 \langle \dot{X}_1^A \dot{X}_2^B \dot{X}_3^C e^{i\delta^{ab}\boldsymbol{k}_a\cdot\boldsymbol{X}_b} \rangle, \tag{41}$$

with $\dot{X}_a^A = \dot{X}^A(\sigma_a)$, $a, b \in \{1, 2, 3\}$, and $\boldsymbol{k}_1 + \boldsymbol{k}_2 + \boldsymbol{k}_3 = 0$. With the Gaussian assumption, the ensemble average of the string observables is lengthy but straightforward. Defining

$$C^{ABC} \equiv \dot{X}_1^A \dot{X}_2^B \dot{X}_3^C, \qquad D \equiv \delta^{ab}\boldsymbol{k}_a \cdot \boldsymbol{X}_b, \tag{42}$$

we have

$$\langle C^{ABC} e^{iD} \rangle = i\langle C^{ABC} D \rangle e^{-(1/2)\langle D^2 \rangle}, \tag{43}$$

and hence

$$B(\boldsymbol{k}_1, \boldsymbol{k}_2, \boldsymbol{k}_3) = -\epsilon^3 \frac{1}{\mathcal{A}} \frac{k_{1_A} k_{2_B} k_{3_C}}{k_1^2 k_2^2 k_3^2} \times \int d\sigma_1 d\sigma_2 d\sigma_3 \langle C^{ABC} D \rangle e^{-(1/2)\langle D^2 \rangle}. \tag{44}$$

We first evaluate the correlator

[1] We thank B. Wandelt for explaining this point to us.

$$\langle C^{ABC}D\rangle = \langle \dot{X}_1^A \dot{X}_2^B \dot{X}_3^C \boldsymbol{k}^a \cdot \boldsymbol{X}_a\rangle$$
$$= \langle \dot{X}_1^A \dot{X}_2^B\rangle\langle \dot{X}_3^C \boldsymbol{k}^a \cdot \boldsymbol{X}_a\rangle + \langle \dot{X}_3^C \dot{X}_1^A\rangle\langle \dot{X}_2^B \boldsymbol{k}^a \cdot \boldsymbol{X}_a\rangle$$
$$+ \langle \dot{X}_2^B \dot{X}_3^C\rangle\langle \dot{X}_1^A \boldsymbol{k}^a \cdot \boldsymbol{X}_a\rangle. \quad (45)$$

The velocity correlators have already been given in Eq. (10). The mixed correlators are most easily evaluated using variations on the theme

$$\boldsymbol{k}^a \cdot \boldsymbol{X}_a = \boldsymbol{k}_1 \cdot (\boldsymbol{X}_1 - \boldsymbol{X}_3) + \boldsymbol{k}_2 \cdot (\boldsymbol{X}_2 - \boldsymbol{X}_3)$$
$$= \boldsymbol{k}_1 \cdot \boldsymbol{X}_{13} + \boldsymbol{k}_2 \cdot \boldsymbol{X}_{23}, \quad (46)$$

where $\boldsymbol{X}_{ab} \equiv \boldsymbol{X}_a - \boldsymbol{X}_b$. For example,

$$\langle \dot{X}_1^A \boldsymbol{k}^a \cdot \boldsymbol{X}_a\rangle = k_2^D\langle \dot{X}_1^A X_{21}^D\rangle + k_3^D\langle \dot{X}_1^A X_{31}^D\rangle. \quad (47)$$

Using the definition of the correlator $\Pi(\sigma)$ in Eq. (17),

$$\langle \dot{X}_1^A \boldsymbol{k}^a \cdot \boldsymbol{X}_a\rangle = \tfrac{1}{2}k_2^A\Pi(\sigma_{21}) + \tfrac{1}{2}k_3^A\Pi(\sigma_{31}), \quad (48)$$

where $\sigma_{ab} = \sigma_a - \sigma_b$. Substituting for the velocity correlators

$$\langle C^{ABC}D\rangle = \tfrac{1}{4}\delta^{AB}[k_1^C\Pi(\sigma_{13}) + k_2^C\Pi(\sigma_{23})]V(\sigma_{12})$$
$$+ \tfrac{1}{4}\delta^{CA}[k_1^B\Pi(\sigma_{12}) + k_3^B\Pi(\sigma_{32})]V(\sigma_{31})$$
$$+ \tfrac{1}{4}\delta^{BC}[k_2^A\Pi(\sigma_{21}) + k_3^A\Pi(\sigma_{31})]V(\sigma_{23}). \quad (49)$$

Now we evaluate

$$\langle D^2\rangle = \langle(\boldsymbol{k}^a \cdot \boldsymbol{X}_a)^2\rangle = \langle(\boldsymbol{k}_1 \cdot \boldsymbol{X}_{13} + \boldsymbol{k}_2 \cdot \boldsymbol{X}_{23})^2\rangle$$
$$= \tfrac{1}{2}k_1^2\Gamma(\sigma_{13}) + \tfrac{1}{2}k_2^2\Gamma(\sigma_{23}) + \boldsymbol{k}_1 \cdot \boldsymbol{k}_2\langle \boldsymbol{X}_{13} \cdot \boldsymbol{X}_{23}\rangle. \quad (50)$$

It can be shown that

$$\langle \boldsymbol{X}_{13} \cdot \boldsymbol{X}_{23}\rangle = \tfrac{1}{2}[\Gamma(\sigma_{13}) + \Gamma(\sigma_{23}) - \Gamma(\sigma_{12})], \quad (51)$$

hence

$$\langle D^2\rangle = -\tfrac{1}{2}[\boldsymbol{k}_1 \cdot \boldsymbol{k}_3\Gamma(\sigma_{13}) + \boldsymbol{k}_2 \cdot \boldsymbol{k}_3\Gamma(\sigma_{23})$$
$$+ \boldsymbol{k}_1 \cdot \boldsymbol{k}_2\Gamma(\sigma_{12})]. \quad (52)$$

Note that this expression is symmetric under the interchange of any pair $\{\sigma_a, \sigma_b\}$ and $\{\boldsymbol{k}_a, \boldsymbol{k}_b\}$. Contracting Eq. (44) with $k_1^A k_2^B k_3^C$, and defining

$$\kappa_{ab} \equiv -\boldsymbol{k}_a \cdot \boldsymbol{k}_b, \quad (53)$$

we have

$$B(\boldsymbol{k}_1, \boldsymbol{k}_2, \boldsymbol{k}_3) = -\epsilon^3 \frac{1}{\mathcal{A}} \frac{1}{4k_1^2k_2^2k_3^2} \int d\sigma_1 d\sigma_2 d\sigma_3 \{\kappa_{12}[\kappa_{13}\Pi(\sigma_{13}) + \kappa_{23}\Pi(\sigma_{23})]V(\sigma_{12}) + \kappa_{13}[\kappa_{12}\Pi(\sigma_{12})$$
$$+ \kappa_{23}\Pi(\sigma_{32})]V(\sigma_{31}) + \kappa_{23}[\kappa_{12}\Pi(\sigma_{21}) + \kappa_{13}\Pi(\sigma_{31})]V(\sigma_{23})\}$$
$$\times \exp\left\{-\frac{1}{4}[\kappa_{13}\Gamma(\sigma_{13}) + \kappa_{23}\Gamma(\sigma_{23}) + \kappa_{12}\Gamma(\sigma_{12})]\right\}. \quad (54)$$

We perform the integrations over the string coordinates σ_a in the Appendix, where it is found

$$B(\boldsymbol{k}_1, \boldsymbol{k}_2, \boldsymbol{k}_3) = -\epsilon^3\pi c_0 \frac{\bar{v}^2}{\bar{t}^4} \frac{L\hat{\xi}}{\mathcal{A}} \frac{1}{\hat{\xi}^2} \frac{1}{k_1^2k_2^2k_3^2}$$
$$\times \left[\frac{k_1^4\kappa_{23} + k_2^4\kappa_{31} + k_3^4\kappa_{12}}{(\kappa_{23}\kappa_{31} + \kappa_{12}\kappa_{31} + \kappa_{12}\kappa_{23})^{3/2}}\right]. \quad (55)$$

This is our primary expression for the bispectrum induced by the GKS effect in cosmic strings. It is proportional to $(GU)^3$, and therefore goes as the $3/2$ power of the power spectrum. The factor $L\hat{\xi}/\mathcal{A}$ is a geometrical factor of order unity, as the projected string length per unit area is of the order of the projected correlation length $\hat{\xi}$ (unless there are a large number of string networks which do not interact with each other). The factor in curly brackets is geometrical in Fourier space, depending on the relative lengths and angles of the $\boldsymbol{k}_a$. The overall dependence on angular quantities is therefore $\hat{\xi}^{-2}k^{-6}$. The dependence on string correlators appears through $\bar{t}$, $\bar{v}^2$, and c_0 defined in Eqs. (22)–(25). This last is an interesting quantity as it is not time reversal invariant: hence the bispectrum could vanish only if the string network is time symmetric. In an expanding universe, the existence of an asymmetry is ensured by decay of the string network. It was argued at the end of Sec. II C that c_0 should be positive.

F. Symmetrical triangle configurations

Current analysis of the CMB temperature bispectrum focuses essentially on a particular local model of primordial non-Gaussianity as well as specific configurations of the primordial bispectrum wave numbers. From Eq. (55), we can easily estimate the string induced bispectrum for various symmetrical triangle configurations in Fourier space. Let us stress that Eq. (55) is the CMB temperature bispectrum as opposed to a primordial bispectrum which is the three point functions of the primordial Newtonian potential, usually of inflationary origin. The latter has still to be evolved through the CMB transfer functions. As a

result, even for identical wave number configurations in Fourier space, the resulting temperature bispectra are not the same.

1. Isosceles triangle

We now consider isosceles triangle configurations in Fourier space such that

$$|\boldsymbol{k}_1| = |\boldsymbol{k}_2| = k, \qquad |\boldsymbol{k}_3| = 2k\sin\frac{\theta}{2}, \tag{56}$$

where θ denotes the angle between the wave vectors $\boldsymbol{k}_1$ and $\boldsymbol{k}_2$. The cross scalar products simplify to

$$\kappa_{12} = k^2\cos\theta, \qquad \kappa_{23} = \kappa_{31} = 2k^2\sin^2(\theta/2), \tag{57}$$

and the isosceles bispectrum reads

$$B_{\rm iso}(k,\theta) = -\epsilon^3\pi c_0\frac{\bar{v}^2}{\bar{t}^4}\frac{L\hat{\xi}}{\mathcal{A}}\frac{1}{\hat{\xi}^2k^6}\frac{1+4\cos\theta\sin^2(\theta/2)}{\sin^3\theta}. \tag{58}$$

Notice that for $\theta = \pi/3$, we obtain the peculiar case of an equilateral triangle [see Eq. (64)]. In Fig. 2, we plotted the angle dependency of the isosceles bispectrum. Such a configuration diverges in the two flat triangle limits for which either $\theta \to 0$ or $\theta \to \pi$. Both of these configurations are therefore better suited than the equilateral one to characterize the strings and are discussed in the next sections. Notice also the change of sign which occurs for the angle

$$\theta_0 = 2\arccos\frac{\sqrt{3-\sqrt{3}}}{2}. \tag{59}$$

For $\theta < \theta_0$, one has $B_{\rm iso} < 0$ (as, for example, in the equilateral configuration), whereas for $\theta > \theta_0$ the bispectrum $B_{\rm iso} > 0$.

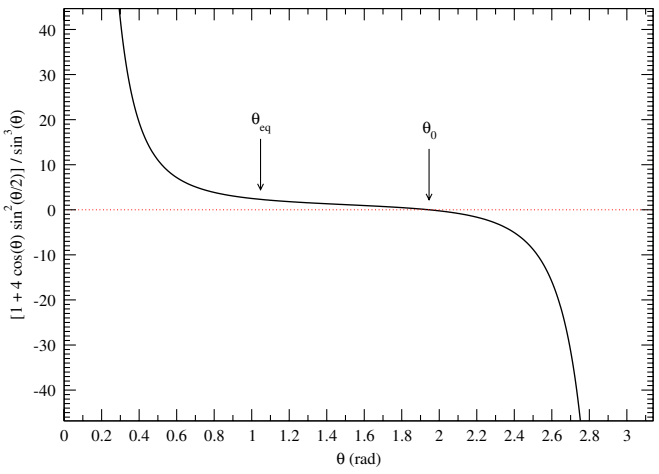

FIG. 2 (color online). Angular dependency of the isosceles bispectrum as a function of the angle θ in between the wave vectors $\boldsymbol{k}_1$ and $\boldsymbol{k}_2$. The particular values $\theta_{\rm eq} = \pi/3$ corresponding to the equilateral configuration as θ_0 at which the bispectrum vanishes are represented. Notice the divergences for flat triangle configurations at $\theta \to 0$ (squeezed) and $\theta \to \pi$ (collapsed).

2. Squeezed triangles

This is the case of one of the sides of the triangle vanishing $k_3 \to k\theta$, with the opposite angle $\theta \to 0$. The angular factor in Eq. (58) simplifies to $1/\theta^3$ and

$$B_{kk\theta} \equiv \lim_{\theta\to 0} B_{\rm iso}(k,\theta) \sim_{\theta\to 0} -\epsilon^3\pi c_0\frac{\bar{v}^2}{\bar{t}^4}\frac{L\hat{\xi}}{\mathcal{A}}\frac{1}{\hat{\xi}^2k^6}\frac{1}{\theta^3}. \tag{60}$$

The bispectrum is therefore negative and appears to diverge in the squeezed limit. In practice, it is not possible to observe such a divergence as the maximum value of the wave vector is bounded by the detector resolution, and the minimum by the map size. Let us also recap that the above calculation breaks down at low wave numbers, and thus for the too small values of θ, since the GKS effect would no longer be the dominant source of temperature anisotropies. It is unclear at what ℓ this happens, but we note that there is no sign of an ℓ^{-1} power law in [34], so the GKS effect may be a subdominant contribution to the cosmic string power spectrum for $\ell < 1500$.

3. Collapsed triangles

There is however another flat triangle configuration for which all wave numbers scale similarly. For $\theta \to \pi$, we have a collapsed triangle with $k_1 = k_2 = k$ and $k_3 \to 2k$. Denoting by

$$\varphi \equiv \pi - \theta, \tag{61}$$

the isosceles bispectrum reduces to

$$B_{k\varphi\varphi} \equiv \lim_{\theta\to\pi} B_{\rm iso}(k,\theta) \sim_{\varphi\to 0} +\epsilon^3 3\pi c_0\frac{\bar{v}^2}{\bar{t}^4}\frac{L\hat{\xi}}{\mathcal{A}}\frac{1}{\hat{\xi}^2k^6}\frac{1}{\varphi^3}. \tag{62}$$

Notice the divergence but with a positive bispectrum. Again, such a divergence is not observable in a realistic situation due to the finite detector resolution. Nevertheless, flat triangles should provide the best framework for the search of a string bispectrum signature. In fact, the change of sign in between the squeezed and collapsed triangles is also of interest to improve the signal to noise ratio. Substracting these two configurations with the appropriate angles should enhance the string signal over the noise.

4. Equilateral triangles

For completeness, we give the bispectrum in the particular case $\theta = \pi/3$, where the $\boldsymbol{k}_a$ are arranged in an equilateral triangle:

$$|\boldsymbol{k}_1| = |\boldsymbol{k}_2| = |\boldsymbol{k}_3| = k. \tag{63}$$

One has $\kappa_{ab} = k^2/2$, and the factor in the squared brackets

in Eq. (55) becomes $4/\sqrt{3}$. As a result,

$$B_{kkk} \equiv B_{\rm eq}(\boldsymbol{k}_1, \boldsymbol{k}_2, \boldsymbol{k}_3) = -\epsilon^3 \frac{4\pi}{\sqrt{3}} c_0 \frac{\bar{v}^2}{\bar{t}^4} \frac{L\hat{\xi}}{\mathcal{A}} \frac{1}{\hat{\xi}^2 k^6}. \quad (64)$$

With $c_0 > 0$, such a configuration produces a negative bispectrum decaying as $1/k^6$ but with an overall amplitude significantly smaller than the collapsed and squeezed triangle configurations.

III. NUMERICAL ESTIMATE

In this section, we directly compute the three point function in Fourier space from a set of 300 CMB temperature maps induced by cosmic strings in the flat sky approximation. These maps have been obtained along the lines of Ref. [24] from Nambu-Goto numerical simulations in FLRW spacetime. As detailed in this reference, they are obtained from the GKS effect using Eq. (4), and are therefore valid on small angular scales only. In the next sections, we briefly recall the numerical method used to generate the maps and then discuss our bispectrum estimator.

A. Nambu-Goto numerical simulations

Our FLRW numerical simulations are based on an improved version of the Bennett and Bouchet Nambu-Goto cosmic string code [24,35,36]. The runs are performed in a comoving box with periodic boundary conditions and whose volume has been scaled to unity. The horizon size $d_{\rm h_0}$ is a free parameter controlling the initial string energy within a horizon volume. For the simulations we performed, $d_{\rm h_0} \simeq 0.185$. The string network is assumed to come from Vachaspati-Vilenkin initial conditions for which the long strings path is a random walk of correlation length $\ell_{\rm c}$, plus a random transverse velocity component of root mean squared amplitude 0.1 [37]. These parameters are set as in Ref. [24] to minimize the relaxation time of the Vachaspati-Vilenkin string network toward its stable cosmological configuration. The temperature maps are then produced according to the GKS effect generated by the strings intercepting our past light cone, using Eq. (4)

$$\Theta \simeq \frac{8\pi i G U}{\boldsymbol{k}^2} \int_{X \cap x_\gamma} (\boldsymbol{u} \cdot \boldsymbol{k}) e^{-i\boldsymbol{k}\cdot\boldsymbol{X}} e^{-\tau} \epsilon d\sigma, \quad (65)$$

where $\tau(\boldsymbol{X})$ is the optical depth to the position of the string, along the line of sight $\hat{\boldsymbol{n}}$, and

$$\boldsymbol{u} = \dot{\boldsymbol{X}} - \frac{(\hat{\boldsymbol{n}} \cdot \boldsymbol{X}') \cdot \boldsymbol{X}'}{1 + \hat{\boldsymbol{n}} \cdot \dot{\boldsymbol{X}}}. \quad (66)$$

The cosmic string simulations are used to compute $\boldsymbol{u}$, based on the string trajectories $\boldsymbol{X}$. The map generation procedure introduces one additional parameter which is the redshift at which we start the simulations $z_{\rm i}$. It has been set to the last scattering surface, namely, $z_{\rm i} = 1089$, and in a flat ΛCDM universe, using fiducial values for the density parameters compatible with the three-year Wilkinson Microwave Anisotropy Probe (WMAP) data [38], corresponding to a numerical comoving box of $L_{\rm sim} \simeq 1.7$ Gpc. Such a size subtends an angle of $\theta_{\rm fov} \simeq 7.2°$ in the sky. The Nambu-Goto simulations and the associated CMB maps therefore depend on only two parameters: the string energy per unit length U, and the initial correlation length $\ell_{\rm c}$. The dependence on $\ell_{\rm c}$ should drop out at late times, as the network is believed to approach a self-similar or scaling configuration. However, in a real Nambu-Goto simulation, there is still some nonscaling structure evident on the smallest length scales [24]. As an illustration example, a typical CMB temperature anisotropy map is represented in Fig. 3, together with the seeding strings projected on our past light cone. We have used our numerical simulations to

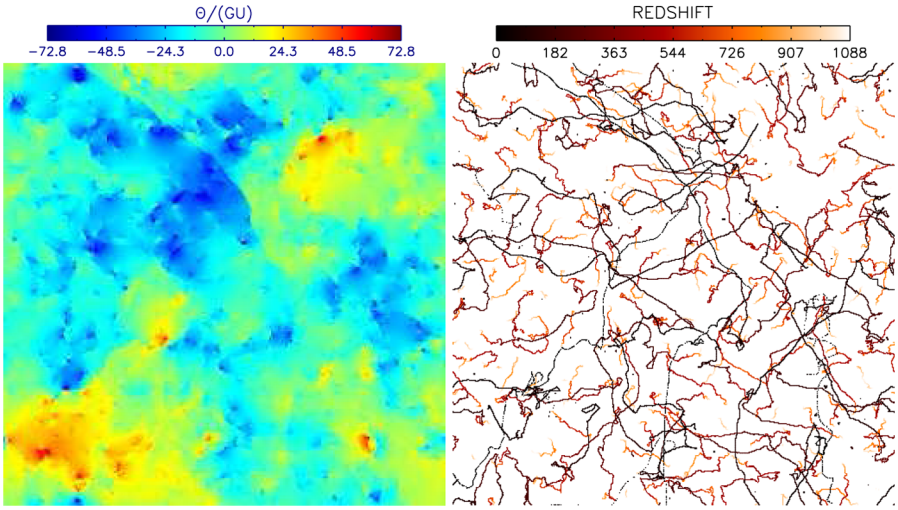

FIG. 3 (color online). Typical CMB temperature map on a 7.2° field (resolution of $\theta_{\rm res} = 0.42'$, $n^2_{\rm pix} = 1024^2$) obtained from Nambu-Goto cosmic string simulations (left panel). The right panel traces back the strings projected on our past light cone.

create 300 statistically independent temperature maps from which one can construct a bispectrum estimator.

B. Reduced bispectrum estimator

1. Scale convolution method

The bispectrum computations use the scale convolution method introduced in Ref. [27] and applied to the flat sky approximation in Ref. [39]. This method relies on the choice of unity window functions in Fourier space $W_u(k)$ peaked around a particular wave number u. Defining

$$\Theta_u(\boldsymbol{x}) \equiv \int \frac{d\boldsymbol{k}}{(2\pi)^2} \hat{\Theta}_{\boldsymbol{k}} W_u(k) e^{-i\boldsymbol{k}\cdot\boldsymbol{x}}, \tag{67}$$

one can construct an estimator of the three point function in Fourier space by remarking that

$$\int \Theta_{k_1}(\boldsymbol{x})\Theta_{k_2}(\boldsymbol{x})\Theta_{k_3}(\boldsymbol{x})d\boldsymbol{x} = \int \frac{d\boldsymbol{p}d\boldsymbol{q}d\boldsymbol{k}}{(2\pi)^6} \hat{\Theta}_{\boldsymbol{p}}\hat{\Theta}_{\boldsymbol{q}}\hat{\Theta}_{\boldsymbol{k}} W_{k_1}(p) \times W_{k_2}(q)W_{k_3}(k)(2\pi)^2 \times \delta(\boldsymbol{p}+\boldsymbol{q}+\boldsymbol{k}). \tag{68}$$

For peaked enough window functions, $\hat{\Theta}_{\boldsymbol{k}}$ remains constant over the window functions width and we construct our reduced bispectrum estimator as

$$b_{k_1k_2k_3} = \frac{1}{S^{(w)}_{k_1k_2k_3}} \left\langle \int \Theta_{k_1}(\boldsymbol{x})\Theta_{k_2}(\boldsymbol{x})\Theta_{k_3}(\boldsymbol{x})d\boldsymbol{x} \right\rangle, \tag{69}$$

where the function $S^{(w)}$ is the flat sky equivalent of the inverse Wigner-3j symbols and reads

$$S^{(w)}_{k_1k_2k_3} = \int \frac{d\boldsymbol{p}d\boldsymbol{q}}{(2\pi)^4} W_{k_1}(p)W_{k_2}(q)W_{k_3}(|\boldsymbol{p}+\boldsymbol{q}|). \tag{70}$$

As noted in Ref. [39], S is of geometrical nature and needs to be computed only once. However, at small angular scales, S is generically a four-dimensional integral whose computation can be time consuming for the large wave numbers. For thin enough window functions, it is nevertheless possible to derive an analytical approximation. Assuming that $W_u(k) = 1$ for $u - w/2 < k < u + w/2$, and zero otherwise, for small enough width w one has

$$W_u(k) \simeq w\delta(k-u). \tag{71}$$

With $\boldsymbol{k}_1$, $\boldsymbol{k}_2$, and $\boldsymbol{k}_3$ forming a triangle, Eq. (70) can be exactly integrated and one finds

$$S^{(w)} \simeq \left(\frac{w}{2\pi}\right)^3 \frac{4k_1k_2k_3}{\sqrt{[(k_1+k_2)^2 - k_3^2][k_3^2 - (k_1-k_2)^2]}}. \tag{72}$$

As can be checked in Fig. 4, the analytical approximation of $S^{(w)}_{k_1k_2k_3}$ given in Eq. (72) is particularly accurate for the large wave numbers. This approach ends up being numerically convenient since it requires only three Fourier transforms to compute the $\Theta_k(\boldsymbol{x})$, together with an integration over all map pixels.

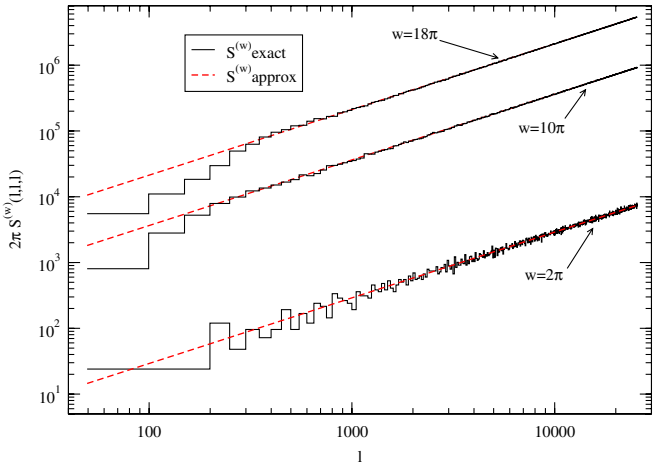

FIG. 4 (color online). Exact versus approximated geometrical $S^{(w)}_{\ell\ell\ell}$ factors for a map with 1024^2 pixels and various choices of the window function with w ($w = 2\pi$ corresponds to one Fourier mode per bandwidth). For large values of w, the deviations for the small multipoles come from the averaging effect. For the small angles we are interested in, Eq. (72) provides a good approximation to the exact expression (70).

2. Statistical averaging and numerical tests

From the previous discussion, the bispectrum is extracted and averaged over the 300 statistical independent maps and for the various triangle configurations discussed in Sec. II F. Our results are presented in the next section. The variance of the bispectrum over the different maps is used to provide an estimate of the statistical errors associated with our approach. Notice however, as discussed at length in Ref. [24], the Nambu-Goto string simulation also leads to some systematic errors due to the nonscaling structure. This can be greatly reduced by eliminating some of the small loops from the network. In order to check our numerical bispectrum estimator, we have performed two tests. The first was to generate a set of synthetic non-Gaussian CMB temperature maps from the non-Gaussian probability distribution

$$P_{\alpha,\sigma}(\Theta) = \frac{e^{-\Theta^2/(2\sigma^2)}}{\sqrt{2\pi}\sigma}\left[\sqrt{1-\alpha^2} + \frac{\alpha}{\sqrt{48}} H_3\left(\frac{\Theta}{\sqrt{2}\sigma}\right)\right], \tag{73}$$

where H_3 stands for the third Hermite polynomial. As shown in Refs. [40,41], such a statistic leads to a reduced bispectrum whose amplitude is given

$$\frac{b_{\ell_1\ell_2\ell_3}}{\sqrt{C_{\ell_1}C_{\ell_2}C_{\ell_3}}} = \frac{1}{n_{\rm pix}} \frac{\mu_3}{\mu_2^{3/2}}, \tag{74}$$

where $\mu_2 = \sigma^2(1+6\alpha^2)$ and $\mu_3 = (2\sigma^2)^{3/2}\alpha\sqrt{3(1-\alpha^2)}$ are the second and third central moments, respectively. It is

not difficult to show that $\mu_3/\mu_2^{3/2}$ is maximized for $\alpha^2 = (7-\sqrt{43})/6$. In Fig. 5, we have plotted the bispectrum obtained from the scale convolution method averaged over 100 of such non-Gaussian ΛCDM temperature maps together with its analytical expectation. At small scales, and up to the statistical errors, the non-Gaussian signal is recovered with the right amplitude. Notice that the loss of power for the low multipoles is simply an artifact coming from the choice of a large window function width ($w = 42\pi$). This necessarily introduces a lower frequency cutoff around $\ell_w \simeq w/\theta_{\rm fov} \simeq 1050$, and also close to the Nyquist frequency (not visible on the plots). As discussed in the following, increasing the values of w reduces the variance of the bispectrum estimator (simply by increasing the number of equivalent triangle configurations in Fourier space probed by the window functions) at the price of losing information for the lower multipoles and those close to the Nyquist frequency. The second test we performed was to integrate the cosmic string bispectrum over all possible triangle configurations such as to check that we indeed recovered the skewness of the string temperature anisotropies. Averaged over the 300 string maps, we found the mean sample skewness to be negative

$$g_1 \equiv \left\langle \frac{\overline{(\Theta-\bar{\Theta})^3}}{\sigma^3} \right\rangle \simeq -0.22 \pm 0.12, \qquad (75)$$

where the brackets stand for the mean over different realizations while the bar denotes averaging on each map. The variance itself averages to

$$\sigma^2 = \langle \overline{(\Theta-\bar{\Theta})^2} \rangle \simeq (150.7 \pm 18)(GU)^2. \qquad (76)$$

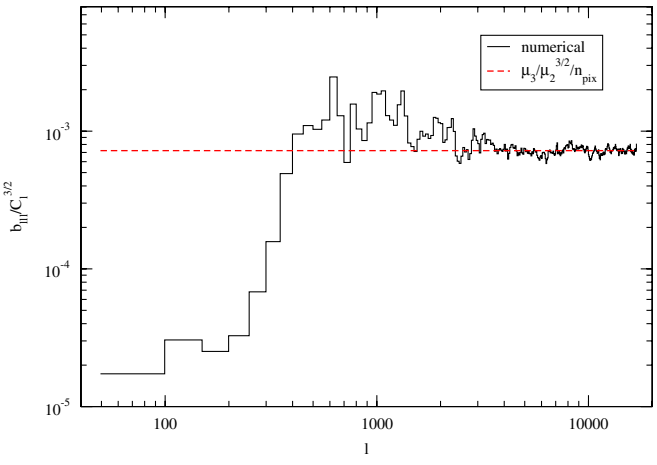

FIG. 5 (color online). The reduced bispectrum computed by the scale convolution method and averaged over 100 of non-Gaussian synthetic ΛCDM temperature maps whose probability distribution function is given by Eq. (73). The red dashed line is the expected non-Gaussian signal. The missing power for low multipoles comes from the cutoff at $\ell_w \simeq w/\theta_{\rm fov} \simeq 1050$ introduced by the choice of large w values for the window functions. The quoted errors are statistical and refer to the square root of the variance between the different realizations.

C. Flat triangle configurations

The previously described method has been applied to extract the isosceles bispectra in the flat triangle configurations for which the amplitude is maximal.

1. Squeezed triangle

Let us first consider the triangle configuration in the squeezed limit such that

$$k_1 = k_2 = k, \qquad k_3 \simeq k\theta, \qquad (77)$$

that we refer to as $\ell\ell\theta$. The mean values of $b_{\ell\ell\theta}$ over the different maps have been plotted in Fig. 6 and for various values of the squeezed angle θ. As found analytically, the bispectrum is negative while the overall amplitude is found to be enhanced by a factor $1/\theta^3$. We have used a window function width equal to $w = 10\pi$ for this plot. However, due to the finite field of view, we cannot go to a very small squeezed angle without truncating the lower modes. From Eq. (77), the lowest multipole achievable is therefore given by

$$\ell_{\rm min} = \frac{w}{\theta_{\rm fov}\theta}, \qquad (78)$$

where the window function cutoff has also been included.

In order to determine the power-law behavior of the bispectrum, we have plotted in Fig. 7 the mean value and standard deviation over the 300 different maps of the squeezed bispectrum for the particular angle $\theta = 0.2$ rad. The variance has been reduced as far as we could by using a large window function width $w = 30\pi$. This explains the

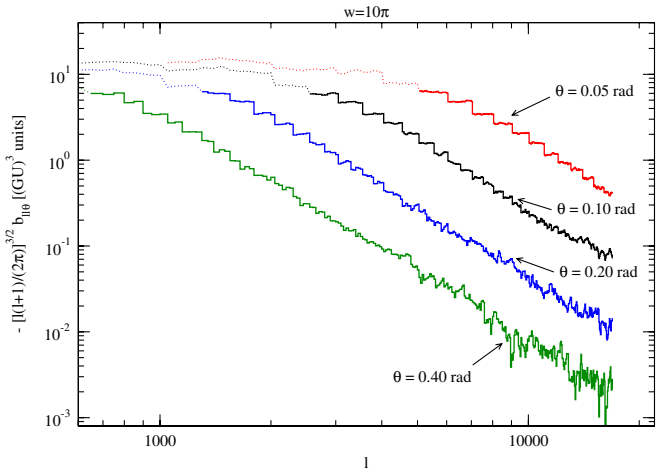

FIG. 6 (color online). Squeezed angle dependency of the mean squeezed bispectrum $[\ell(\ell+1)/(2\pi)]^{3/2} b_{\ell\ell\theta}$. The spurious plateau (dotted lines) for the lower multipoles comes from the cutoff associated with a given squeezed angle θ together with the window function width w and occurs at $\ell_{\rm min} = w/(\theta_{\rm fov}\theta)$.

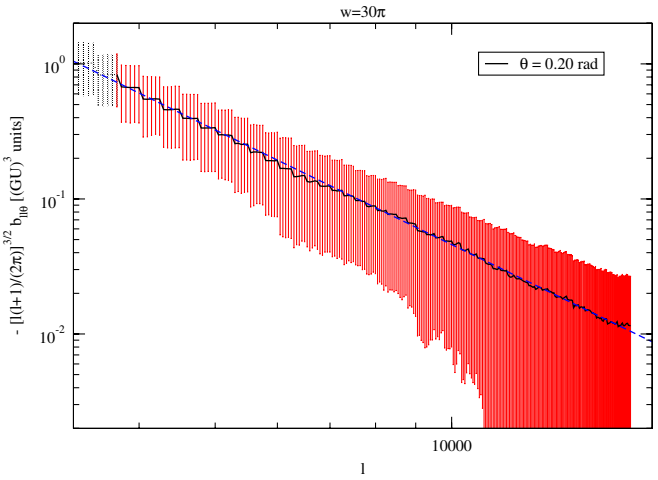

FIG. 7 (color online). Mean value and standard deviation of the squeezed bispectrum $[\ell(\ell+1)/(2\pi)]^{3/2}b_{\ell\ell\theta}$ for $\theta = 0.2$ rad. The window function width has been increased to $w = 30\pi$ to reduce the variance pushing up the lower multipole cutoff to $\ell_{\rm min} = w/(\theta_{\rm fov}\theta) \simeq 3750$. The dashed line is the best power-law fit whose power has been set to the one obtained from the equilateral configuration [see Eq. (84)].

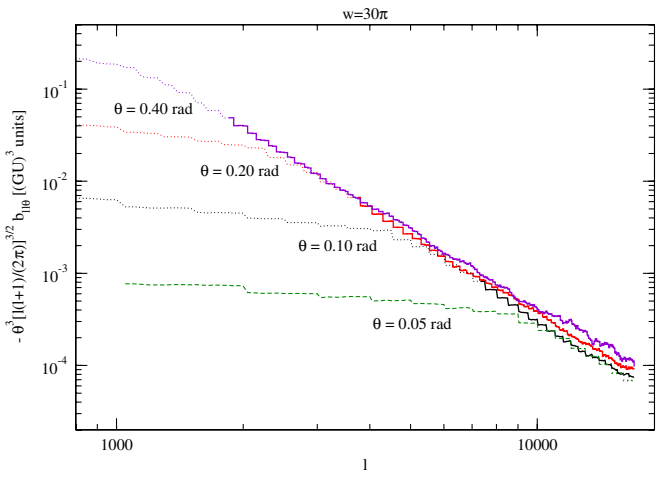

FIG. 8 (color online). Rescaled mean squeezed bispectrum $\theta^3[\ell(\ell+1)/(2\pi)]^{3/2}b_{\ell\ell\theta}$ showing the $1/\theta^3$ dependency. Notice the large window function width $w = 30\pi$ chosen to reduce the statistical errors and pushing up the numerical multipole cutoff $l_{\rm min}$.

low multipole cutoff at a quite large value of $\ell_{\rm min} \simeq 3750$. A power-law fit against the mean numerical estimator for $\ell > \ell_{\rm min}$ and truncated at $\ell_{\rm max} = 16\,000$ gives

$$[\ell(\ell+1)]^{3/2}b_{\ell\ell\theta} \propto_{\ell\gg1} \ell^{-q} \quad \text{with} \quad q = 2.82. \tag{79}$$

We do not quote error bars since this value is relatively sensitive to the choice of $\ell_{\rm max}$ and, as can been seen in Fig. 7, the standard deviation of our estimator becomes an order of magnitude bigger than the bispectrum itself for $\ell > 16\,000$.

The power dependency of Eq. (79) is remarkably close to the analytical expectation. In fact, the noninteger value for the power may be expected due to the fractal properties of the Nambu-Goto strings [23]. As shown in Ref. [24], the power spectrum itself was found to behave as

$$\ell(\ell+1)C_\ell \propto_{\ell\gg1} \ell^{-p} \quad \text{with} \quad p = 0.889. \tag{80}$$

From Eqs. (79) and (80), we the find the analytical power-law behavior of the ratio

$$\frac{b_{\ell\ell\theta}}{C_\ell^{3/2}} \propto_{\ell\gg1} \ell^{-(q-3p/2)} \quad \text{with} \quad q - \frac{3}{2}p = 1.49. \tag{81}$$

The dashed blue line in Fig. 7 is the best power-law fit ℓ^{-q}.

The $1/\theta^3$ dependency of the squeezed bispectrum is illustrated in Fig. 8. Again, to reduce the variance, the width has been set to $w = 30\pi$ and we have plotted $\theta^3[\ell(\ell+1)/(2\pi)]^{3/2}b_{\ell\ell\theta}$ for the four θ values of Fig. 6. As expected, all rescaled mean values match their respective multipole cutoff $\ell_{\rm min}$ [see Eq. (78)].

Concerning the overall amplitude, it can be evaluated around the minimum variance multipole and we find at $\ell =$ 5000

$$[\ell(\ell+1)/(2\pi)]^{3/2}b_{\ell\ell\theta} \simeq (-2.7 \pm 1.4) \times 10^{-3}\left(\frac{GU}{\theta}\right)^3. \tag{82}$$

To conclude this section, the squeezed bispectrum is found to follow the analytical results of Sec. II, up to the noninteger power-law behavior with respect to the multipole moment which may be interpreted as a fractal effect associated with the Nambu-Goto string small-scale structure.

2. Collapsed triangles

As discussed in Sec. II F 3, the collapsed triangles correspond to the limit $\varphi \to 0$ for the isosceles configuration and to the mode values

$$k_1 = k_2 = k, \qquad k_3 \simeq 2k. \tag{83}$$

The scale convolution method is hardly applicable in this case since all collapsed triangles fitting in the window function width will be indistinguishable. Although this averaging effect allowed us to increase the statistics for the squeezed triangle configurations, for the collapsed ones one can no longer assume that the bispectrum is constant over the window function, especially since it diverges in the limit $\varphi \to 0$. As a result, w has been kept to a low value ($w = 3\pi$) and the modes have been binned to reduce the statistical errors. As can be seen in Fig. 9, our numerical estimation does not allow to accurately trace the bispectrum down to the small values of φ. Nevertheless, we do observe the change of sign for $\varphi \to 0$ albeit at a smaller value than the one predicted analytically.

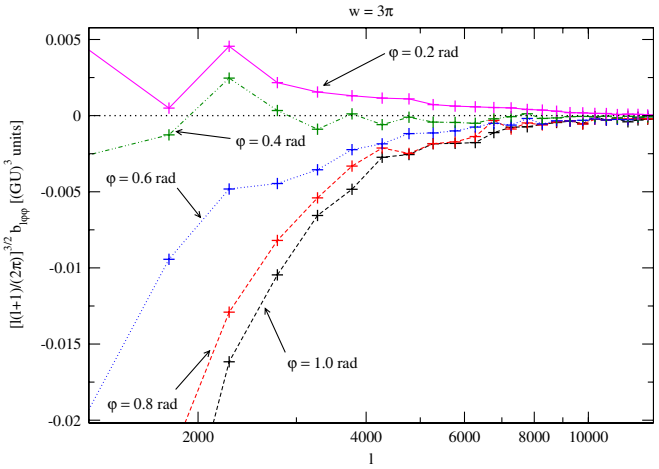

FIG. 9 (color online). Mean collapsed bispectrum $[\ell(\ell+1)/(2\pi)]^{3/2} b_{\ell\varphi\varphi}$. This configuration is extremely sensitive to the window function properties and statistical errors dominate. The change of sign for small values of φ is nevertheless observable.

D. Equilateral configurations

The previously described method has also been applied to extract the equilateral bispectrum $b_{\ell\ell\ell}$. In Fig. 10, we have plotted its mean value over the 300 different maps as well as its standard deviation. To reduce the variance of the estimator we have chosen $w = 30\pi$ which gives a low multipole cutoff $\ell_w \simeq 750$. The equilateral bispectrum is of smaller amplitude than the squeezed one, and its numerical determination is quite challenging. It is however clear from this plot that $b_{\ell\ell\ell} < 0$ in agreement with the analytical results of Sec. II.

A power-law fit against the mean numerical estimator over the range of multipoles $\ell_w < \ell < \ell_{\rm max}$, with $\ell_{\rm max} = 16\,000$, gives the same power as for the squeezed triangle configurations, namely,

$$[\ell(\ell+1)]^{3/2} b_{\ell\ell\ell} \propto_{\ell\gg 1} \ell^{-q} \quad \text{with} \quad q = 2.82. \tag{84}$$

Concerning the overall amplitude, we find at $\ell = 1000$

$$[\ell(\ell+1)/(2\pi)]^{3/2} b_{\ell\ell\ell} \simeq (-0.53 \pm 0.3)(GU)^3, \tag{85}$$

which is again of the same order of magnitude as our analytical estimate. Using the power-law fit, such an amplitude can be extrapolated up to $\ell = 5000$ and compared to Eq. (82). In particular, we recover, up to the statistical errors, the analytical result

$$\frac{b_{\ell\ell\ell}}{\theta^3 b_{\ell\ell\theta}} = \frac{4}{\sqrt{3}}. \tag{86}$$

For completeness, the above ratio has been plotted for $\theta = 0.2$ rad in Fig. 11.

As can be seen in Fig. 10, but also in Fig. 7, the bispectrum decays faster than its standard deviation at small scales. This can be understood by using the nearly Gaussian approximation in which the non-Gaussian trispectrum is neglected. Under these assumptions, the variance of the bispectrum estimator, for the equilateral configurations, is given by [39,42]

$$\sigma_b^2 = \frac{6}{S^{(w)}_{\ell\ell\ell}} C_\ell^3. \tag{87}$$

Using Eq. (72), one gets

$$\sigma_b = \sqrt{\frac{2\pi}{\theta_{\rm fov}}} \left(\frac{2\pi}{w}\right)^{3/2} \left[\frac{27}{4\ell(\ell+1)}\right]^{1/4} \left[\frac{\ell(\ell+1)C_\ell}{2\pi}\right]^{3/2}. \tag{88}$$

As expected, the variance is reduced by a factor w^3 coming from the different numbers of equivalent triangle configurations probed by window functions of width w. From

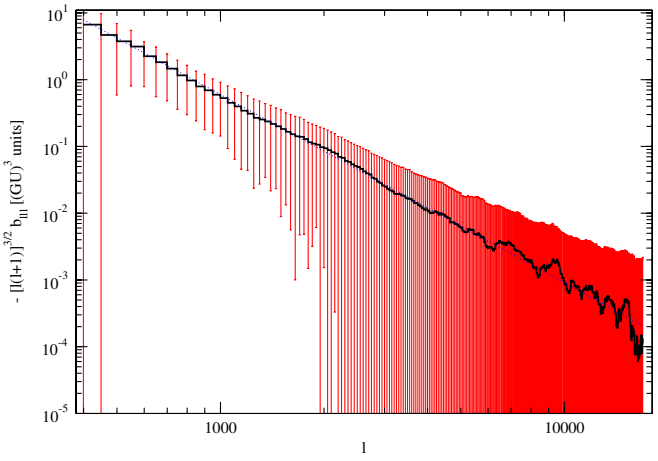

FIG. 10 (color online). Mean and standard deviation of the equilateral bispectrum $[\ell(\ell+1)/(2\pi)]^{3/2} b_{\ell\ell\ell}$ over our 300 string temperature maps and obtained for window function width $w = 30\pi$. The blue dotted line is the power-law fit of Eq. (84).

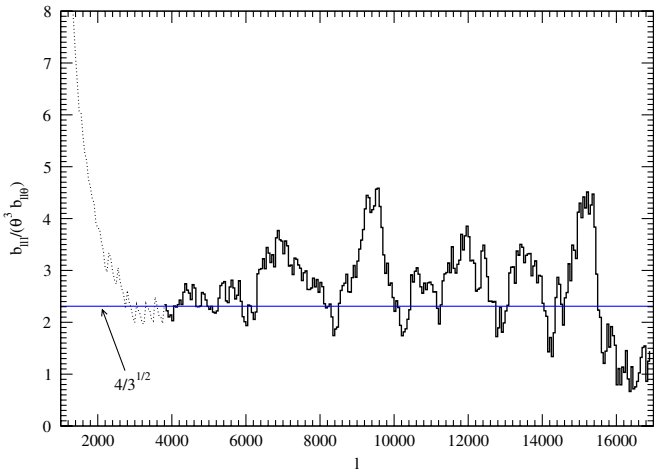

FIG. 11 (color online). Ratio of the mean bispectra $b_{\ell\ell\ell}/(\theta^3 b_{\ell\ell\theta})$ obtained for $\theta = 0.2$ rad. Up to the statistical errors, the expected value $4/\sqrt{3}$ is recovered for $\ell > \ell_{\rm min}$.

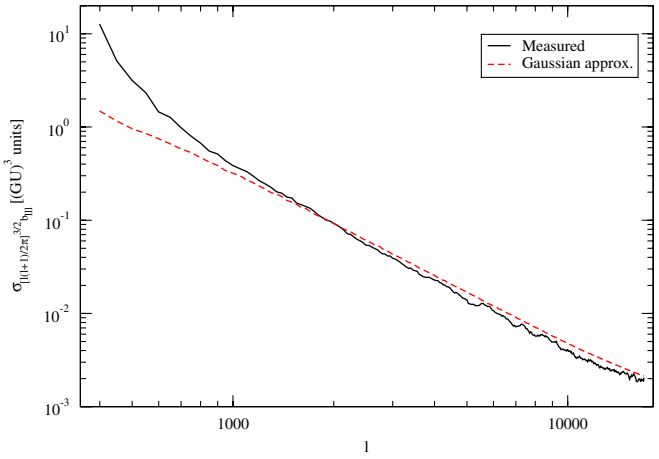

FIG. 12 (color online). Standard deviation of the bispectrum estimator over the 300 string temperature maps (black solid curve) compared with the nearly Gaussian random expected standard deviation obtained from Eq. (88).

Eqs. (80) and (88), one gets $\sigma_b \propto \ell^{-4.83}$ which vanishes slower than the bispectrum estimator at large multipoles. In Fig. 12, we plotted the standard deviation obtained from Eq. (88), relying only on the mean string power spectrum, together with the measured standard deviation of our bispectrum estimator. There is good agreement for both the power-law behavior and the overall amplitude. From this section, we conclude that although the cosmic string equilateral bispectrum is nonvanishing, its measurement at small angles may be difficult due to its fast decay compared to the associated standard deviation. This is also the case for the squeezed and collapsed configurations, but with the former being of higher amplitude, this should be less problematic.

IV. COMPARISON WITH DATA

From both the analytical and numerical results, the cosmic string bispectra associated with the flat triangle configurations are the best suited to look for string signatures. However, it is not easy to compare with existing bispectrum estimates as much of the literature focuses on particular local models of primordial non-Gaussianity in which the Newtonian potential is parametrized [43]

$$\Phi(\boldsymbol{x}) = \Phi(\boldsymbol{x})_{\mathrm{L}} + f_{\mathrm{NL}}^{\mathrm{loc}}[\Phi_{\mathrm{L}}^2(\boldsymbol{x}) - \langle\Phi_{\mathrm{L}}^2(\boldsymbol{x})\rangle]. \quad (89)$$

The local type of primordial non-Gaussianity produces a bispectrum whose maximal amplitude occurs for squeezed triangle configurations, as is the case for the cosmic strings. However, as a result of the CMB transfer functions, a given value of $f_{\mathrm{NL}}^{\mathrm{loc}}$ corresponds to oscillating damped patterns of the CMB temperature bispectrum, which are therefore completely different from the power law we have derived for the strings at small scales. The current bounds on $f_{\mathrm{NL}}^{\mathrm{loc}}$, being precisely obtained from template matching procedures, cannot be applied to the string bispectrum [17,29]. Notice that the analyses concerned with the other type of primordial non-Gaussianities, such as the equilateral ones characterized by $f_{\mathrm{NL}}^{\mathrm{eq}}$, are also affected by the CMB transfer function [17] and cannot straightforwardly be compared to our findings.

However, a simple calculation we can do at this stage is, at a given angular scale, to compare the overall amplitude of the CMB bispectrum induced by a primordial $f_{\mathrm{NL}}^{\mathrm{loc}}$ with the one induced by the presence of cosmic strings. For simplicity, let us choose the equilateral configuration (which is not of maximal amplitude for both the strings and local primordial non-Gaussianity). With the Cosmic Background Explorer normalized CMB temperature fluctuations, and neglecting Silk damping, Ref. [43] gives the amplitude of the oscillating CMB bispectrum induced by primordial non-Gaussianity:

$$\max|B_{lll}| \simeq (2 \times 10^{-17}) l^{-4} |f_{\mathrm{NL}}^{\mathrm{loc}}|. \quad (90)$$

We can now estimate the size of the equilateral bispectrum from strings if they contribute about 10% of the temperature power spectrum at $\ell = 10$. In this case $\epsilon \simeq 2 \times 10^{-5}$, and assuming Abelian Higgs strings where $GU \simeq 0.7 \times 10^{-6}$ [14,44], one has

$$B_{kkk} \simeq -(4 \times 10^{-14}) c_0 \frac{\bar{v}^2}{\bar{t}^4} \frac{L\hat{\xi}}{\mathcal{A}} \frac{1}{\hat{\xi}^2 k^6} \left(\frac{GU}{0.7 \times 10^{-6}}\right)^3. \quad (91)$$

Matching the two suggests that string fluctuations may generate a temperature bispectrum at $\ell \simeq 500$ as large as the one that would be produced by a local $|f_{\mathrm{NL}}^{\mathrm{loc}}|$ of around 10^3 ($k\hat{\xi} \simeq 1$ is near the peak of the scalar modes at $\ell \sim 500$). This number should be considered as an order of magnitude estimate since the string bispectrum calculation is only accurate for higher ℓ, while Eq. (90) is applicable for $\ell \leq 1000$ [43]. Let us also mention that this value for $f_{\mathrm{NL}}^{\mathrm{loc}}$ is only valid at $\ell \simeq 500$ and does not represent the value that would be obtained by a local primordial bispectrum template matching against the string bispectrum. In order to obtain such a value, one should perform a Fisher matrix analysis over all the multipoles along the lines of Refs. [45,46]. Such an analysis is outside the scope of this paper and we leave it for a forthcoming work.

V. CONCLUSION

We have analytically and numerically derived the CMB temperature bispectrum induced by cosmic strings from the Gott-Kaiser-Stebbins effect. This effect is the main source of string induced CMB anisotropies at small angle and our result is applicable at those angular scales only. The bispectrum is negative for equilateral and all isosceles squeezed configurations, having a power-law decay close to ℓ^{-6}. The squeezed isosceles bispectrum is significantly amplified for small squeezing angle by a factor θ^{-3}. Although the vanishing limit is forbidden by any finite detector resolution, one should expect the ongoing and

future high resolution CMB experiment to be more sensitive to these signatures [47–49]. The collapsed isosceles configuration still exhibits the same power law, an angle dependency in φ^{-3} (with $\varphi = \pi - \theta$) but leads to a positive bispectrum. This feature could allow an enhancement of the string signal by subtracting the bispectrum of these two configurations. The numerically measured amplitudes have been given in the text and, at the particular scale $\ell = 500$, they roughly correspond to a $|f_{\rm NL}^{\rm loc}| \simeq 10^3$ for the local type of primordial non-Gaussianity in the equilateral configurations. This number is for illustrative purpose only and should be treated with caution. First, the temperature bispectrum induced by the strings has a different multipole dependency than the one coming from primordial non-Gaussianities. As a result, the value for $f_{\rm NL}^{\rm loc}$ quoted above is definitely not the one that would be obtained by applying a primordial bispectrum template matching over the actual string bispectrum. In particular, the current bounds derived so far on the primordial $f_{\rm NL}$ values do not apply for the strings. Moreover, even at the string prediction level, there are competing and correlated effects at this angular scale, notably the acoustic oscillations that we have not considered here. Nevertheless, this value for $f_{\rm NL}^{\rm loc}$ shows that this is an interesting angular scale to search for string non-Gaussianity and that devoted string template matching should be used in the search of CMB non-Gaussian signals.

Finally, as the power-law dependence of the bispectrum variance may suggest, we should expect an even stronger non-Gaussian signal from the cosmic string trispectrum and we leave its analysis for a forthcoming work.

ACKNOWLEDGMENTS

This work is partially supported by the Belgian Federal Office for Scientific, Technical, and Cultural Affairs through the Inter-University Attraction Pole Grant No. P6/11. The cosmic string simulations have been performed thanks to computing support provided by the Planck-HFI processing center at the Institut d'Astrophysique de Paris.

APPENDIX: STRING COORDINATE INTEGRATIONS

In this Appendix we perform the integrals over the string coordinates σ_a in the expression (55) for the bispectrum. We repeat the expressions for convenience:

$$B(\boldsymbol{k}_1, \boldsymbol{k}_2, \boldsymbol{k}_3) = -\epsilon^3 \frac{1}{\mathcal{A}} \frac{k_{1_A} k_{2_B} k_{3_C}}{k_1^2 k_2^2 k_3^2} \times \int d\sigma_1 d\sigma_2 d\sigma_3 \langle C^{ABC} D \rangle e^{-(1/2)\langle D^2 \rangle}, \tag{A1}$$

where

$$k_{1_A} k_{2_B} k_{3_C} \langle C^{ABC} D \rangle e^{-(1/2)\langle D^2 \rangle} = \tfrac{1}{4}\{\kappa_{12}[\kappa_{13}\Pi(\sigma_{13}) + \kappa_{23}\Pi(\sigma_{23})]V(\sigma_{12}) + \kappa_{13}[\kappa_{12}\Pi(\sigma_{12}) + \kappa_{23}\Pi(\sigma_{32})]V(\sigma_{31}) + \kappa_{23}[\kappa_{12}\Pi(\sigma_{21}) + \kappa_{13}\Pi(\sigma_{31})]V(\sigma_{23})\} \exp\{-\tfrac{1}{4}[\kappa_{13}\Gamma(\sigma_{13}) + \kappa_{23}\Gamma(\sigma_{23}) + \kappa_{12}\Gamma(\sigma_{12})]\}. \tag{A2}$$

Thanks to the symmetry identified earlier, there is essentially only one integral to do, as the six terms in Eq. (55) are related by a permutation symmetry. We can define a function of three variables

$$F(\kappa_{12}, \kappa_{23}, \kappa_{31}) = \int d\sigma_1 d\sigma_2 d\sigma_3 \Pi(\sigma_{13}) V(\sigma_{12}) \times \exp\left\{\frac{1}{4}[-\kappa_{31}\Gamma(\sigma_{13}) - \kappa_{23}\Gamma(\sigma_{23}) - \kappa_{12}\Gamma(\sigma_{12})]\right\}, \tag{A3}$$

in terms of which

$$k_1^A k_2^B k_3^C \langle C^{ABC} D \rangle e^{-(1/2)\langle D^2 \rangle} = \tfrac{1}{4}\{\kappa_{12}\kappa_{31}F(\kappa_{12}, \kappa_{23}, \kappa_{31}) + \kappa_{12}\kappa_{23}F(\kappa_{12}, \kappa_{31}, \kappa_{23}) + \kappa_{31}\kappa_{12}F(\kappa_{31}, \kappa_{23}, \kappa_{12}) + \kappa_{31}\kappa_{23}F(\kappa_{31}, \kappa_{12}, \kappa_{23}) + \kappa_{23}\kappa_{12}F(\kappa_{23}, \kappa_{31}, \kappa_{12}) + \kappa_{23}\kappa_{31}F(\kappa_{23}, \kappa_{12}, \kappa_{31})\}. \tag{A4}$$

A change of coordinates simplifies the integration:

$$\sigma_{123} = \tfrac{1}{3}(\sigma_1 + \sigma_2 + \sigma_3), \tag{A5}$$

giving

$$F(\kappa_{12}, \kappa_{23}, \kappa_{31}) = \int d\sigma_{123} d\sigma_{12} d\sigma_{31} \Pi(\sigma_{31}) V(\sigma_{12}) \times \exp\left\{\frac{1}{4}[-\kappa_{31}\Gamma(\sigma_{31}) - \kappa_{23}\Gamma(\sigma_{23}) - \kappa_{12}\Gamma(\sigma_{12})]\right\}, \tag{A6}$$

where we have used $\Pi(\sigma_{31}) = \Pi(\sigma_{13})$ and $\Gamma(\sigma_{31}) = \Gamma(\sigma_{13})$. Inserting the identity

$$1 = \int d\sigma_{23} \delta(\sigma_{23} + \sigma_{12} + \sigma_{31}), \tag{A7}$$

and using an integral representation for the δ function we have

$$F(\kappa_{12}, \kappa_{23}, \kappa_{31}) = L \int \frac{d\lambda}{2\pi} \int d\sigma_{12} d\sigma_{23} d\sigma_{31} \Pi(\sigma_{31}) V(\sigma_{12}) \times \exp[i\lambda(\sigma_{23} + \sigma_{12} + \sigma_{31})] \times \exp\left\{-\frac{1}{4}[\kappa_{13}\Gamma(\sigma_{31}) + \kappa_{23}\Gamma(\sigma_{23}) + \kappa_{12}\Gamma(\sigma_{12})]\right\}. \tag{A8}$$

Hence we can factorize

$$F(\kappa_{12}, \kappa_{23}, \kappa_{31}) = L \int \frac{d\lambda}{2\pi} I(\lambda, \kappa_{12}) J(\lambda, \kappa_{23}) K(\lambda, \kappa_{31}), \tag{A9}$$

where

$$I(\lambda, \kappa_{12}) = \int d\sigma V(\sigma) e^{i\lambda\sigma - (1/4)\kappa_{12}\Gamma(\sigma)}, \tag{A10}$$

$$J(\lambda, \kappa_{23}) = \int d\sigma e^{i\lambda\sigma - (1/4)\kappa_{23}\Gamma(\sigma)}, \tag{A11}$$

$$K(\lambda, \kappa_{31}) = \int d\sigma \Pi(\sigma) e^{i\lambda\sigma - (1/4)\kappa_{31}\Gamma(\sigma)}. \tag{A12}$$

We evaluate I, J, and K for small angles. For κ_{ab} large and positive, and assuming the relevant limits for the correlation functions

$$\Gamma(\sigma) \simeq \bar{t}^2 \sigma^2, \qquad V(\sigma) \simeq \bar{v}^2, \qquad \Pi(\sigma) \simeq \frac{1}{2} \frac{c_0}{\hat{\xi}} \sigma^2, \tag{A13}$$

one gets

$$I(\lambda, \kappa_{12}) \simeq \frac{\bar{v}^2}{\bar{t}} \sqrt{\frac{4\pi}{\kappa_{12}}} \exp\left(-\frac{\lambda^2}{\kappa_{12}\bar{t}^2}\right), \tag{A14}$$

$$J(\lambda, \kappa_{23}) \simeq \frac{1}{\bar{t}} \sqrt{\frac{4\pi}{\kappa_{23}}} \exp\left(-\frac{\lambda^2}{\kappa_{23}\bar{t}^2}\right), \tag{A15}$$

$$K(\lambda, \kappa_{31}) \simeq \frac{c_0}{\hat{\xi}} \frac{1}{\kappa_{31}\bar{t}^3} \sqrt{\frac{4\pi}{\kappa_{31}}} \left(1 - \frac{2\lambda^2}{\kappa_{31}\bar{t}^2}\right) \exp\left(-\frac{\lambda^2}{\kappa_{31}\bar{t}^2}\right). \tag{A16}$$

Hence

$$F(\kappa_{12}, \kappa_{23}, \kappa_{31}) \simeq 4\pi L \frac{\bar{v}^2}{\bar{t}^4} \frac{c_0}{\hat{\xi}} \times \frac{\kappa_{23} + \kappa_{12}}{(\kappa_{23}\kappa_{31} + \kappa_{12}\kappa_{31} + \kappa_{12}\kappa_{23})^{3/2}}. \tag{A17}$$

Though we have assumed $\kappa_{ab} > 0$ in deriving this equation, the result is still applicable even if κ_{ab} is negative because the combination $\kappa_{23}\kappa_{31} + \kappa_{12}\kappa_{31} + \kappa_{12}\kappa_{23}$ in the denominator is positive definite. Actually, by using approximations (A13), one can derive (A17) directly from Eq. (A3) which is well defined even for negative κ_{ab} because of the positive definiteness of the exponent. Defining the new function

$$g(\kappa_{12}, \kappa_{23}, \kappa_{31}) = \frac{\kappa_{12} + \kappa_{23}}{(\kappa_{23}\kappa_{31} + \kappa_{12}\kappa_{31} + \kappa_{12}\kappa_{23})^{3/2}}, \tag{A18}$$

we can write

$$B(\boldsymbol{k}_1, \boldsymbol{k}_2, \boldsymbol{k}_3) = -\epsilon^3 \pi c_0 \frac{\bar{v}^2}{\bar{t}^4} \frac{L\hat{\xi}}{\mathcal{A}} \frac{1}{\hat{\xi}^2} \frac{1}{k_1^2 k_2^2 k_3^2} \times \{\kappa_{12}\kappa_{31} g(\kappa_{12}, \kappa_{23}, \kappa_{31}) + \kappa_{12}\kappa_{23} g(\kappa_{12}, \kappa_{31}, \kappa_{23}) + \kappa_{31}\kappa_{12} g(\kappa_{31}, \kappa_{23}, \kappa_{12}) + \kappa_{31}\kappa_{23} g(\kappa_{31}, \kappa_{12}, \kappa_{23}) + \kappa_{23}\kappa_{12} g(\kappa_{23}, \kappa_{31}, \kappa_{12}) + \kappa_{23}\kappa_{31} g(\kappa_{23}, \kappa_{12}, \kappa_{31})\}. \tag{A19}$$

Thanks to g being symmetric in its first two arguments, and using $\kappa_{23} + \kappa_{12} = k_2^2$ (and circular permutations), some simplification follows:

$$B(\boldsymbol{k}_1, \boldsymbol{k}_2, \boldsymbol{k}_3) = -\epsilon^3 \pi c_0 \frac{\bar{v}^2}{\bar{t}^4} \frac{L\hat{\xi}}{\mathcal{A}} \frac{1}{\hat{\xi}^2} \frac{1}{k_1^2 k_2^2 k_3^2} \times \{k_2^2 \kappa_{31} g(\kappa_{12}, \kappa_{23}, \kappa_{31}) + k_1^2 \kappa_{23} g(\kappa_{31}, \kappa_{12}, \kappa_{23}) + k_3^3 \kappa_{12} g(\kappa_{23}, \kappa_{31}, \kappa_{12})\}. \tag{A20}$$

Finally, using the definition of g from Eq. (A18),

$$B(\boldsymbol{k}_1, \boldsymbol{k}_2, \boldsymbol{k}_3) = -\epsilon^3 \pi c_0 \frac{\bar{v}^2}{\bar{t}^4} \frac{L\hat{\xi}}{\mathcal{A}} \frac{1}{\hat{\xi}^2} \frac{1}{k_1^2 k_2^2 k_3^2} \times \frac{k_1^4 \kappa_{23} + k_2^4 \kappa_{31} + k_3^4 \kappa_{12}}{(\kappa_{23}\kappa_{31} + \kappa_{12}\kappa_{31} + \kappa_{12}\kappa_{23})^{3/2}}. \tag{A21}$$

[1] M. B. Hindmarsh and T. W. B. Kibble, Rep. Prog. Phys. **58**, 477 (1995).
[2] A. Vilenkin and E. P. S. Shellard, *Cosmic Strings and Other Topological Defects* (Cambridge University Press, Cambridge, England, 1994).
[3] M. Sakellariadou, Lect. Notes Phys. **718**, 247 (2007).
[4] T. W. B. Kibble, J. Phys. A **9**, 1387 (1976).
[5] A. Dabholkar, G. W. Gibbons, J. A. Harvey, and F. Ruiz Ruiz, Nucl. Phys. **B340**, 33 (1990).
[6] E. J. Copeland, R. C. Myers, and J. Polchinski, J. High Energy Phys. 06 (2004) 013.
[7] J. Yokoyama, Phys. Rev. Lett. **63**, 712 (1989).
[8] L. Kofman, A. D. Linde, and A. A. Starobinsky, Phys. Rev. Lett. **73**, 3195 (1994).
[9] E. J. Copeland, A. R. Liddle, D. H. Lyth, E. D. Stewart, and D. Wands, Phys. Rev. D **49**, 6410 (1994).
[10] R. Jeannerot, J. Rocher, and M. Sakellariadou, Phys. Rev. D **68**, 103514 (2003).
[11] S. Sarangi and S. H. H. Tye, Phys. Lett. B **536**, 185 (2002).
[12] G. Dvali and A. Vilenkin, J. Cosmol. Astropart. Phys. 03 (2004) 010.
[13] R. A. Battye, B. Garbrecht, and A. Moss, J. Cosmol. Astropart. Phys. 09 (2006) 007.
[14] N. Bevis, M. Hindmarsh, M. Kunz, and J. Urrestilla, Phys. Rev. Lett. **100**, 021301 (2008).
[15] A. Gangui, L. Pogosian, and S. Winitzki, Phys. Rev. D **64**, 043001 (2001).
[16] L. Senatore, K. M. Smith, and M. Zaldarriaga, arXiv:0905.3746.
[17] K. M. Smith, L. Senatore, and M. Zaldarriaga, J. Cosmol. Astropart. Phys. 09 (2009) 006.
[18] N. Bevis, M. Hindmarsh, M. Kunz, and J. Urrestilla, Phys. Rev. D **76**, 043005 (2007).
[19] L. Pogosian and M. Wyman, Phys. Rev. D **77**, 083509 (2008).
[20] J. R. Gott III, Astrophys. J. **288**, 422 (1985).
[21] N. Kaiser and A. Stebbins, Nature (London) **310**, 391 (1984).
[22] M. Hindmarsh, S. Stuckey, and N. Bevis, Phys. Rev. D **79**, 123504 (2009).
[23] C. J. A. P. Martins and E. P. S. Shellard, Phys. Rev. D **73**, 043515 (2006).
[24] A. A. Fraisse, C. Ringeval, D. N. Spergel, and F. R. Bouchet, Phys. Rev. D **78**, 043535 (2008).
[25] M. Hindmarsh, Astrophys. J. **431**, 534 (1994).
[26] Keitaro Takahashi, Atsushi Naruko, Yuuiti Sendouda, Daisuke Yamauchi, Chul-Moon Yoo, and Misao Sasaki, arXiv:0811.4698.
[27] D. N. Spergel and D. M. Goldberg, Phys. Rev. D **59**, 103001 (1999).
[28] A. Gangui and J. Martin, Phys. Rev. D **62**, 103004 (2000).
[29] E. Komatsu *et al.* (WMAP Collaboration), Astrophys. J. Suppl. Ser. **180**, 330 (2009).
[30] M. White, J. Carlstrom, M. Dragovan, and W. Holzapfel, Astrophys. J. **514**, 12 (1999).
[31] M. LoVerde and N. Afshordi, Phys. Rev. D **78**, 123506 (2008).
[32] N. Kaiser and A. Stebbins, Nature (London) **310**, 391 (1984).
[33] F. R. Bouchet, D. P. Bennett, and A. Stebbins, Nature (London) **335**, 410 (1988).
[34] N. Bevis, M. Hindmarsh, M. Kunz, and J. Urrestilla, Phys. Rev. D **75**, 065015 (2007).
[35] D. P. Bennett and F. R. Bouchet, Phys. Rev. D **41**, 2408 (1990).
[36] C. Ringeval, M. Sakellariadou, and F. R. Bouchet, J. Cosmol. Astropart. Phys. 02 (2007) 023.
[37] T. Vachaspati and A. Vilenkin, Phys. Rev. D **30**, 2036 (1984).
[38] D. N. Spergel *et al.*, Astrophys. J. Suppl. Ser. **170**, 377 (2007).
[39] N. Aghanim, M. Kunz, P. G. Castro, and O. Forni, Astron. Astrophys. **406**, 797 (2003).
[40] C. R. Contaldi and J. Magueijo, Phys. Rev. D **63**, 103512 (2001).
[41] G. Rocha, M. P. Hobson, S. Smith, P. Ferreira, and A. Challinor, Mon. Not. R. Astron. Soc. **357**, L1 (2005).
[42] N. Bartolo, E. Komatsu, S. Matarrese, and A. Riotto, Phys. Rep. **402**, 103 (2004).
[43] E. Komatsu and D. N. Spergel, Phys. Rev. D **63**, 063002 (2001).
[44] N. Bevis, M. Hindmarsh, M. Kunz, and J. Urrestilla, Phys. Rev. D **75**, 065015 (2007).
[45] E. Sefusatti and E. Komatsu, Phys. Rev. D **76**, 083004 (2007).
[46] D. Nitta, E. Komatsu, N. Bartolo, S. Matarrese, and A. Riotto, J. Cosmol. Astropart. Phys. 05 (2009) 014.
[47] J. Ruhl *et al.* (SPT Collaboration), Proc. SPIE Int. Soc. Opt. Eng. **5498**, 11 (2004).
[48] K. M. Huffenberger and U. Seljak, New Astron. Rev. **10**, 491 (2005).
[49] R. Barker *et al.* (AMI Collaboration), Mon. Not. R. Astron. Soc. **369**, L1 (2006).